VNU Journal of Science: Mathematics - Physics
Journal homepage: https://js.vnu.edu.vn/MaP

Original Article

Preparation of Ag/Au Bimetallic Nanodecahedra through Galvanic Displacement Method

Pham Thi Nga[1,2], Pham Thi Thu Ha[1,*], Nguyen Dac Dien[3], Doan Thi Thao Anh[1,4], Tran Thu Trang[1], Nguyen Vu Anh Tuyet[5], Vuong Truong Xuan[1], Vu Xuan Hoa[1]

[1]*Institute of Science and Technology, TNU-University of Sciences, Tan Thinh, Thai Nguyen, Vietnam*
[2]*Hoa Lu University, 2 Xuan Thanh, Ninh Nhat, Hoa Lu, Ninh Binh, Vietnam*
[3]*Vietnam Trade Union University, 169 Tay Son, Quang Trung, Dong Da, Hanoi, Vietnam*
[4]*Bac Duyen Ha High School, 3 Hung Ha, Hung Ha, Thai Binh, Vietnam*
[6]*Hung Yen High School for the Gifted, 1 Chu Van An, An Ta, Hung Yen, Vietnam*

Received 21st October 2024
Revised 26th November 2024; Accepted 15th February 2025

Abstract: In this work, Ag/Au bimetallic nanodecahedra was successfully synthesized using the reduction process and photochemical method. Polyvinylpyrrolidone was used as a shape-directing agent, $AgNO_3$, $HAuCl_4$ as precursor raw materials, sodium borohydride as a reducing agent for the growth of Ag metal. Ag^+ ions were reduced to Ag nanoparticles (AgNPs) as seeds using sodium borohydride ($NaBH_4$), and then Ag nanodecahedra (AgND) were prepared by a photochemical seeding growth method under the illumination of blue light emitting diode (BLED) with a wavelength of 480 nm. Next, an Au nanofilm was formed by chemical reduction on the surface of the Ag nanodecahedra from precursors of $HAuCl_4$ and ascorbic acid ($C_6H_8O_6$). At the same time, Ag was replaced by Au through a galvanic replacement reaction. As-prepared products have been characterized by X-ray diffraction, scanning electron microscope (SEM), transmission electron microscope (TEM), high-resolution transmission electron microscope (HRTEM), energy dispersive X-ray spectroscopy (EDS), EDX mapping, and ultraviolet-visible (UV-Vis) absorption spectroscopy. The intensity and position of UV-Vis peaks of AgND and Ag/Au changed as BLED illumination time and HAuCl4 amount changed.

Keywords: Au/Ag bimetallic, galvanic replacement reaction, nanodecahedra, photochemical reduction.

1. Introduction

An intrinsic property of metallic nanoparticles is localized surface plasmon resonance (LSPR). It has been widely applied in photothermal therapy [1], medicine [2], biomedicine [3], surface-enhanced

* Corresponding author.
E-mail address: haptt@tnus.edu.vn

https//doi.org/10.25073/2588-1124/vnumap.4972

Raman scattering (SERS) substrates [4], antibacterial [5], etc. The plasmon optical properties of metallic nanoparticles can be modulated by adjusting their shape, size, and composition. Single-element noble metal materials such as gold (Au) and silver (Ag) have some limitations in terms of chemical stability and reproducibility. Although Ag nanostructures were applied in surface-enhanced Raman scattering (SERS) substrates owing to their reusability, biocompatibility, and high SERS performance, their surface is highly sensitive to oxidation, so Ag-based SERS substrates have poor stability. To improve the stability of Ag, an Au thin nanolayer that does not influence the sensitivity of Ag-based SERS substrates has been coated on Ag core. Therefore, coating an Au nanolayer on Ag nanostructure is highly desirable to overcome the drawback of pristine Ag. The combination of Au and Ag to form Au@Ag or Ag@Au core-shell or Ag/Au bimetallic alloy has been reported in numerous works. Core-shell nanostructures contain a metal core surrounded by other metal shell [6]. The position of the localized surface plasmon resonance (LSPR) band has been shifted as the radius of the bimetallic spherical or thickness of the shell increases [7].

For example, Yin et al., prepared Ag@Au core-shell dendrites via a two-step process. Ag dendrites were grown on Si wafer using the hydrothermal corrosion method, and Au nanofilm was then fabricated on the surface of Ag dendritic nanostructure by chemical reduction [8]. Huang et al., synthesized Au@Ag dendritic nanoforests on silicon by fluoride-assisted galvanic replacement reaction method [9]. Yang et al., prepared gold-coated silver (Ag-Au) and silver-coated gold (Au-Ag) composite nanoparticles by a seeding growth method [10]. Pham et al. developed an Au-Ag alloy on SiO_2 nanoparticles, in which $AgNO_3$ was reduced by ascorbic acid and using polyvinylpyrrolidone (PVP) as the structure-directing agent, then Ag shell was grown on the surface of the Au seeds [11]. Fu et al. synthesized Au-Ag alloy nano-garlands with multiple petal-like branches using $HAuCl_4$ and $AgNO_3$ as precursors, ascorbic acid as a reducing agent, and 4-NTP as a shape-directing agent [12]. Liu et al., manufactured Ag core-embedded Au film by thermally depositing Ag/Au alloy target, and the monodisperse Ag nanoparticles were embedded within the Au film [13]. Attila et al., used spark discharge generation in the gas phase to fabricate Au/Ag nanoparticles onto glass microfiber filters [14]. Khan et al. fabricated Au-Ag alloy nanoparticles on filter paper by soaking filter paper in a mixture of $HAuCl_4$ and $AgNO_3$ solution [15]. Lee et al., developed bimetallic Au/Ag nanocavities by galvanic engineering [16]. Liu also prepared Ag-Au bimetals through galvanic replacement reactions [17], etc.

There is still a huge space for developing this kind of Ag/Au bimetallic nanostructure, especially through the galvanic displacement route. Ag nanoparticles were commonly used as sacrificial templates to synthesize alloy nanoparticles. For instance, Wang et al. synthesized Au-Ag nanocages with hollow interiors and porous walls through galvanic replacement using Ag nanocubes as templates [5]. The elemental composition and the shell layer-specific surface area can be controlled by varying the amount of precursors and reaction time [18]. The cell dimension and crystal structure of Au and Ag metals are almost the same. Ag has a higher plasmonic response than Au, but Au has better chemical stability comparing to Ag. Combining Ag and Au leads to better SERS performance than pure Au or Ag nanoparticles.

Herein, we prepared a new bimetallic Ag/Ag nanodecahedra composed of Ag core covered by Au shell with various Au/Ag ratios. The samples were synthesized in two steps containing the photochemical reduction and galvanic replacement reaction using silver nanodecahedra as a sacrificial template to obtain hollow silver-gold alloy nanoshells. The dimension of the hollow cavities can be controlled by varying the amount of $HAuCl_4$. The prepared Ag/Au decahedra can be applied to the SERS analysis.

2. Methods

2.1. Materials

Silver nitrate ($AgNO_3$, 99.98%), trisodium citrate dihydrate (TSC, $Na_3C_6H_5O_7.2H_2O$, 99%), polyvinylpyrrolidone (PVP, molar weight MW = 40,000 g/mol), sodium borohydride ($NaBH_4$, 99%), sodium hydroxide (NaOH, 99%), L-ascorbic acid (L-AA, $C_6H_8O_6$, 99.96%), chloroauric acid ($HAuCl_4.4H_2O$, 99.9%) were purchased from Merck Co. (Germany). All the chemicals were of analytical grade and used as received from the supplier without further purification. Double-distilled water and absolute ethanol were used as solvents for solution preparation and rinsing of prepared products. In this work, Ag was synthesized before Au.

2.2. Preparation of Ag Nanodecahedra

The Ag nanodecahedra was synthesized via a two-step experimental process. In the first step, Ag nanoparticles were prepared using a reduction route. Typically, 2 ml $AgNO_3$ solution (0.01 M), 0.4 ml trisodium citrate (TSC, 0.6 M), and 0.6 ml polyvinylpyrrolidone (PVP, 0.0067 M) were mixed in 150 ml distilled water in an ice bath under continuous stirring for 15 min. The reaction temperature was controlled at 4 °C. Then, 0.5 ml $NaBH_4$ solution (0.1 M) was added dropwise into the above mixture under continuous stirring for 1 hour, and the color of the reaction solution gradually changed to grey-yellow. The Ag^+ ions from $AgNO_3$ were reduced to produce metallic Ag nanoparticles.

$$2AgNO_3 + 2NaBH_4 \rightarrow 2Ag + H_2 \uparrow + 2BH_3 + 2NaNO_3 \quad (1)$$

Afterward, 0.4 ml NaOH solution (0.05 M) was added to the mixture and further stirring for 15 min. In the second step, the growth of Ag nanodecahedra from Ag nanoparticles was performed in a photochemical reaction apparatus. A blue light emitting diode (BLED, wavelength of 480 nm) was used as a stimulating visible light source. The light power was maintained at 22.5 mW, and exposure time was set at 5, 10, 20, 30, 40, 60, and 80 min. The corresponding Ag nanodecahedra were signed as AgND5, AgND10, AgND20, AgND30, AgND40, AgND60, and AgND80, respectively. Ag nanoparticles were self-assembled through a diffusion-limited aggregation process. Ag nanoparticles adhere to form clusters governed by the lowest surface energy, allowing the formation of Ag nanodecahedra. Finally, the obtained products were filtered and washed several times with deionized water and absolute ethanol to remove excess sodium citrate, sodium borohydride remnant, and by-products such as BH_3 and $NaNO_3$. After filtration, the samples were resuspended in deionized water and stirred for 2 h to replace the surfactant (PVP) to achieve Ag nanodecahedra.

2.3. Formation of Au Nanolayer on the Surface of Ag Nanodecahedra

The reaction was carried out at room temperature (20 - 25 °C). Firstly, the full amount of the as-prepared AgND20, 0.4 ml ascorbic acid (L-AA, 0.01 M), and 0.6 ml polyvinylpyrrolidone (PVP, 0.0067 M) were dispersed in 50 ml deionized water using magnetic stirring. Then, 10 µl $HAuCl_4$ with different amounts of 0.15, 0.25, 0.35, 0.45, 0.55, and 0.65 µmol was slowly added into the above mixture under magnetic stirring for 1 hour. The reaction solution changed color abundantly by adjusting the addition of $HAuCl_4$. The obtained Ag/Au bimetallic products were signed as Ag/Au1, Ag/Au2, Ag/Au3, Ag/Au4, Ag/Au5, and Ag/Au6, respectively. Au nanolayer would be formed via the reduction of $HAuCl_4$ by ascorbic acid as the following equation:

$$3C_6H_8O_6 + 20HAuCl_4 + 18H_2O \rightarrow 20Au + 80HCl + 18CO_2 \quad (2)$$

Spontaneously, Ag was replaced by Au through galvanic displacement. Finally, the obtained product was washed with deionized water several times. Fig. 1 illustrates the fabrication process of Ag/Au bimetallic nanodecahedra.

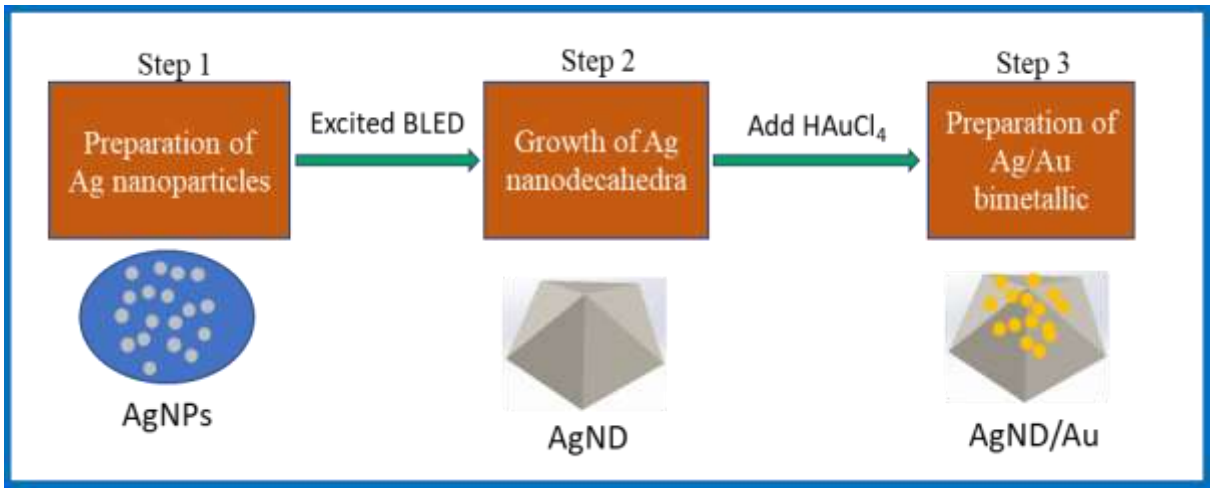

Figure 1. Illustration of Ag nanodecahedra and Ag/Au bimetallic fabrication procedure.

2.4. Characterizations

The phase identification of the samples was characterized via powder X-ray diffraction (XRD, Bruker D8 Advance, Germany) operated at 30 kV with Cu-K_α radiation (wavelength of λ = 0.154056 nm) in the scanning angle 2θ in the range of 30-80°. The morphologies and microstructures were observed via scanning electron microscopy (SEM, Hitachi S4800, Japan) operating at 10 kV, transmission electron microscopy (TEM, JEOL JEM-1010, Japan) operating at 80 kV, high-resolution TEM (HRTEM, JEOL JEM-1010, Japan) operating at 200 kV. A particle size analyzer (Micro 100C, 3P Instruments, Germany) was also utilized to measure the size distribution of samples. The chemical composition was executed by energy-dispersive X-ray spectroscopy (EDS, Nova 450). The elemental distribution in the nanostructures was examined through energy-dispersive X-ray (EDX) spectroscopy mapping (Hitachi SU 8020) operating at an accelerating voltage of 200 kV. The optical properties were monitored by recording the ultraviolet-visible (UV-Vis) absorbance spectra using a UV-Vis spectrophotometer (JASCO V770, Japan) in the wavelength of 200–800 nm.

3. Results and Discussion

3.1. Samples Morphology and Size

Fig. 2a shows a TEM image of AgNPs with homogeneous shapes and good dispersion. The average diameter of the AgNPs is almost 7 nm (Fig. 2b). The TEM image of the Ag nanodecahedra (AgND) before loading Au nanolayer is shown in Fig. 2c. The diameter of AgND is around 80 nm, and the surface is smooth. Figure 2d is a SEM image of Ag/Au bimetallic nanostructure, showing that only nanodecahedra can be clearly seen.

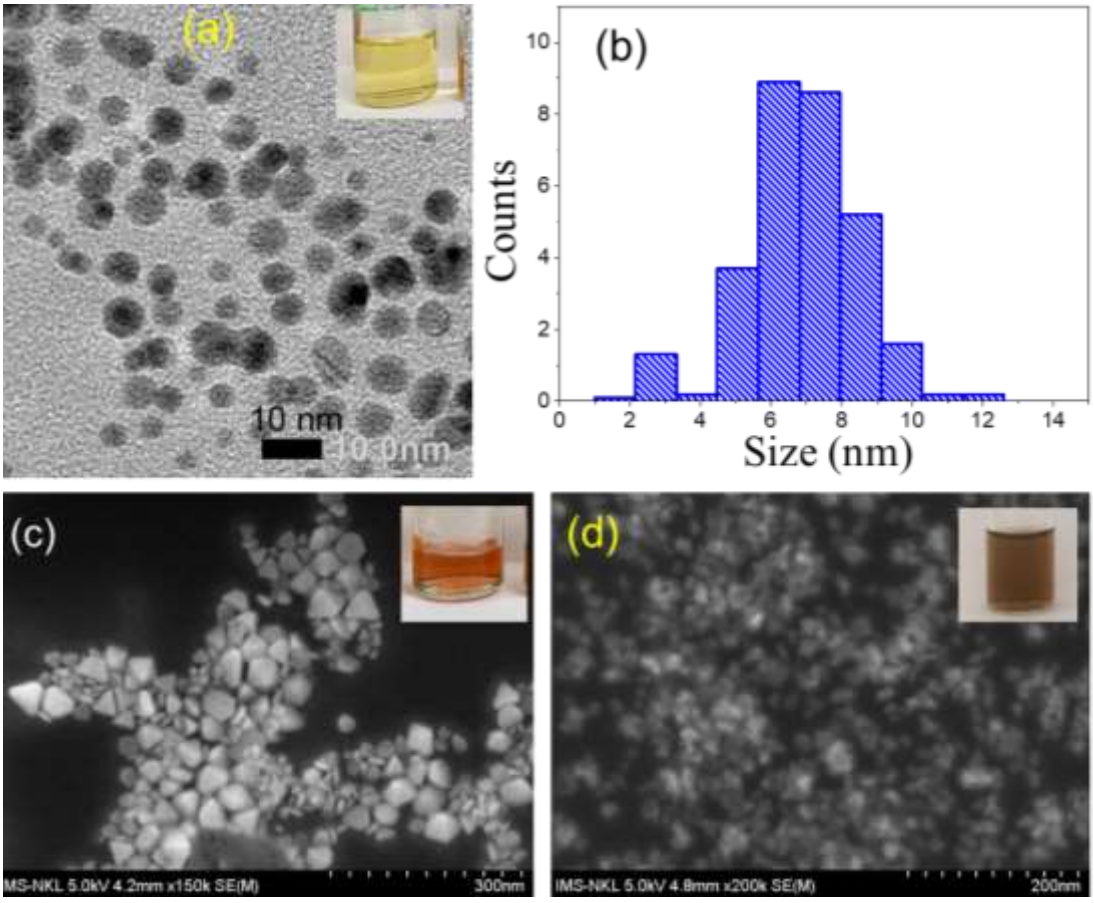

Figure 2. (a) TEM image of Ag nanoparticles, (b) size distribution of Ag seed nanoparticles; (c) SEM image of AgND20, (d) SEM image of Ag/Au bimetallic, insets in (a, c, d) are the corresponding solutions.

After Au^{3+} ions reduction process, an Au nanolayer with a thickness of approximately 4 nm appears on the Ag surface. The size of the Ag/Au bimetallic nanostructure is almost the same as that of the primordial Ag nanodecahedra. To study the effect of $HAuCl_4$ on the formation of bimetallic nanostructure, the different amounts of $HAuCl_4$ (i.e., 0.15, 0.25, 0.35, 0.45, 0.55, and 0.65 µmol) were added into mixture of AgND, L-AA, and PVP. Figure 3a shows that when a small amount (0.15 µmol) $HAuCl_4$ is added, a thin layer is formed, and the arrangement between the nanodecahedra is close and partially overlapping. The nanodecahedra have no obvious hollow cores. When increasing the $HAuCl_4$ amount to 0.35 µmol, the morphology of the nanodecahedra changes dramatically, and adjacent nanodecahedra with internal hollow cavities stacked together, the round edges and apices are instead of sharp ones (Fig. 3c). When the amount of $HAuCl_4$ was increased to 0.55 µmol, the average size of the nanodecahedra increases from 80 to 90 nm due to the formation of Au nanofilms (Fig. 3e). The nanodecahedra become larger and coarser, the gaps between neighboring nanodecahedra decrease. As the Au layer continues to grow, it gradually expands outwards, wrapping around twelve sides to form an almost rounded shell layer. With the increase of the amount of $HAuCl_4$ upto 0.65 µmol, the difference in the shapes and sizes of the nanodecahedra decreases, and they become more uniform. The distribution of nanodecahedra was denser, the overlap between neighboring nanodecahedra increased, the particle size of the nanodecahedra increased, and their sharpness decreased.

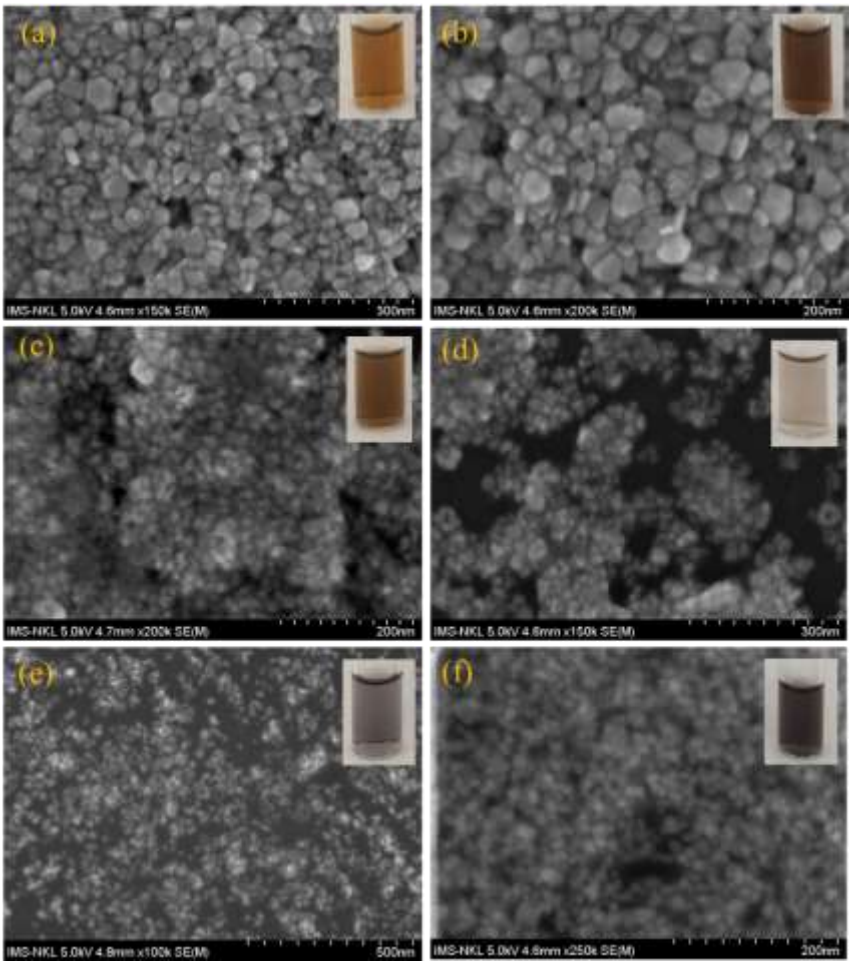

Figure 3. SEM images of Ag/Au formed from different HAuCl4 amounts: (a) Ag/Au1 (0.15 µmol HAuCl4), (b) Ag/Au2 (0.25 µmol HAuCl4), (c) Ag/Au3 (0.35 µmol HAuCl4), (d) Ag/Au4 (0.45 µmol HAuCl4), (e) Ag/Au5 (0.55 µmol HAuCl4), (f) Ag/Au6 (0.65 µmol HAuCl4), insets are the corresponding solutions.

3.2. Crystalline Structure

Fig. 4 shows XRD patterns of Ag nanoparticles, Ag nanodecahedra, and Ag/Au bimetallic nanomaterials. Four diffraction peaks at 37.9°, 44.07°, 63.9°, and 76.7° respectively belong to (111), (200), (220), and (311) crystalline planes of face-centered cubic (FCC) phase Ag or Au (JCPDS no. 71-3752). Both Au and Ag have FCC crystal structures with cell dimensions of 4.07 Å and 4.08 Å, respectively [19]. (111) peak is the most intense and sharp, indicating that the Ag and Au atoms favor to locate along the (111) direction because surface energy is lowest on the (111) crystalline plane. XRD patterns demonstrated the remarkable crystalline of the as-prepared product. Figure 4b shows the dependence of Ag/Au crystal size on $HAuCl_4$ amount, where the crystal size of samples was estimated from the most intense peak of (111) in XRD patterns using Scherrer equation [20]:

$$D = \frac{k\lambda}{\beta \cos\theta} \tag{3}$$

where D is the average crystalline size, $k = 0.893$ is the Scherrer constant, $\lambda = 0.154056$ nm is the CuKα wavelength, β is the full width at half maximum (FWHM) of the diffraction peak, and θ is the Bragg diffraction angle.

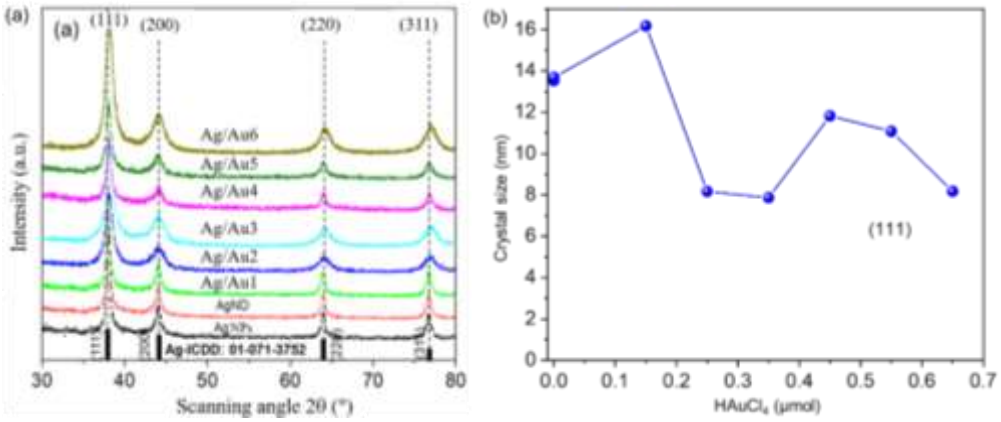

Figure 4. (a) XRD patterns of Ag nanoparticles, Ag nanodecahedra, Ag/Au1-Ag/Au6; (b) Dependence of Ag/Au crystal size on HAuCl4 amount.

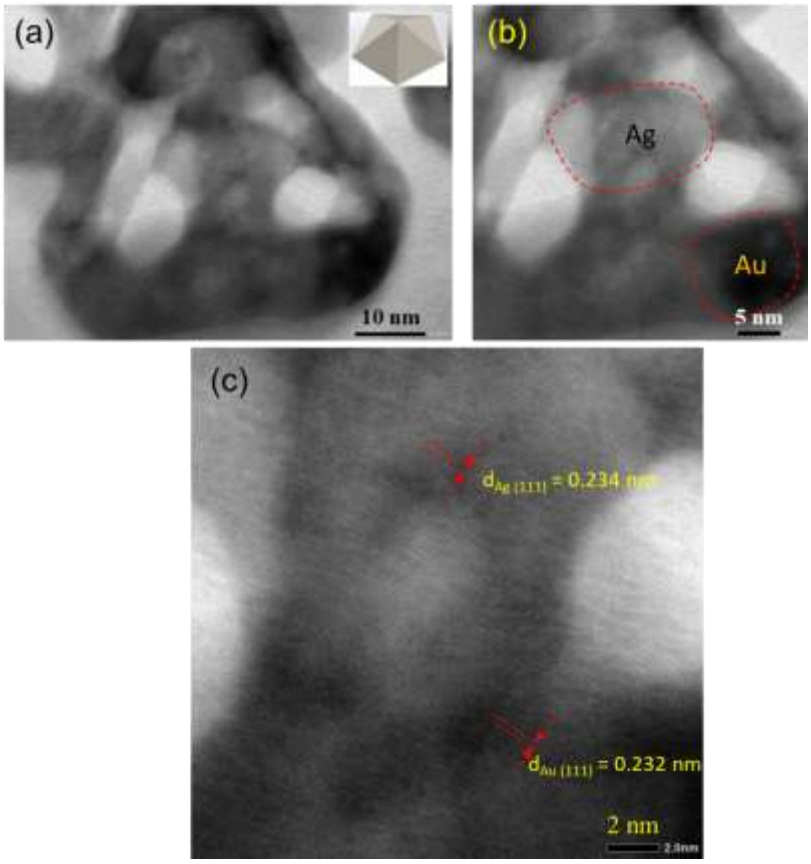

Figure 5. TEM images of (a) Ag/Au1, (b) Ag/Au2, (c) HRTEM of Ag/Au4.

Fig. 5 shows TEM and HRTEM images of an individual Ag/Au nanodecahedra. As verified by the HRTEM result, the Ag and Au have high crystallinity with clear lattice fringes. The lattice fringes of the Ag and Au were about 0.234 nm and 0.232 nm, which correspond to the interplanar spacings of $\{111\}$ of FCC Ag and Au crystals, respectively.

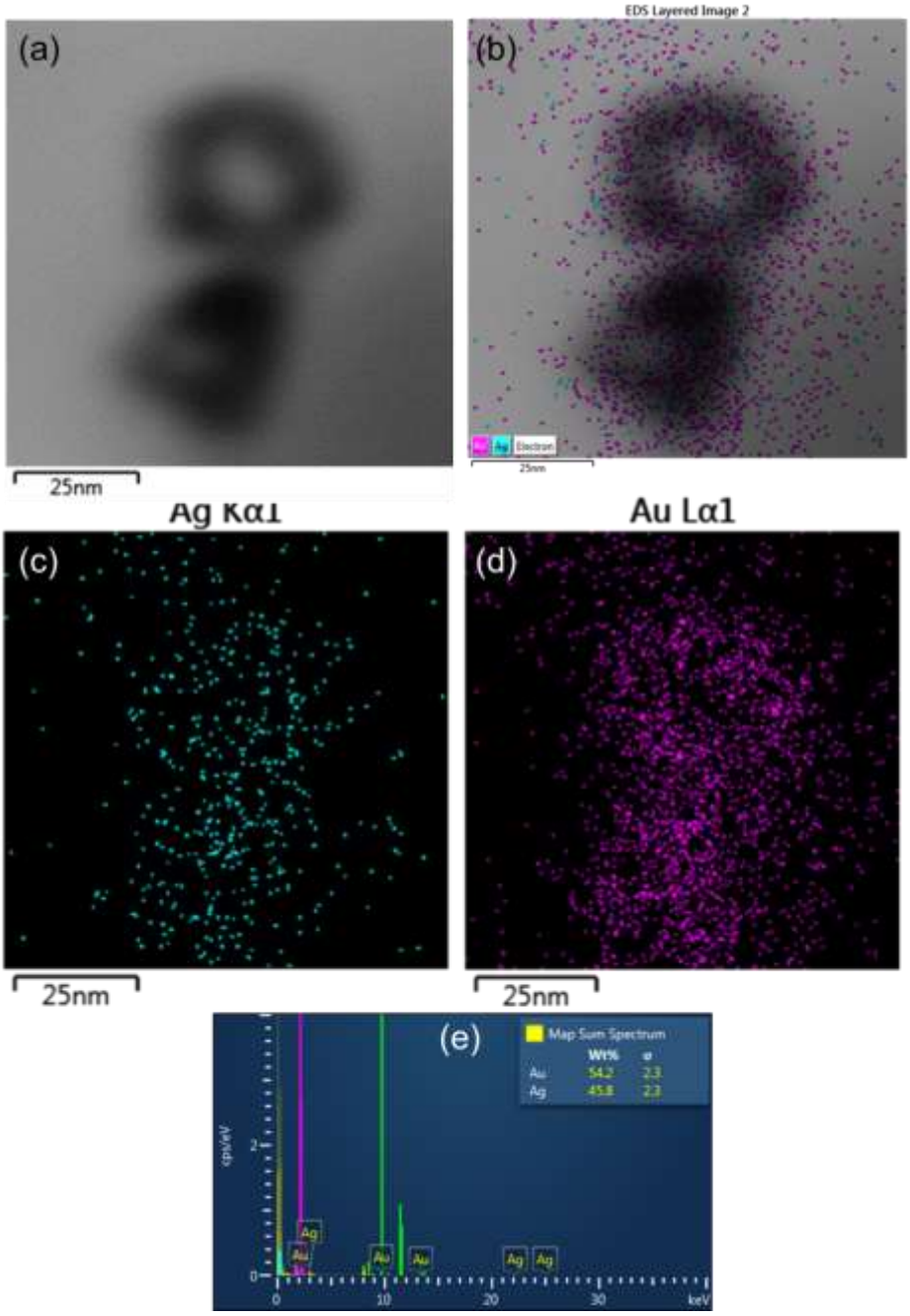

Figure 6. (a-d) EDX elemental mapping of Ag and Au on an Ag/Au nanodecahedra; (e) EDS spectrum of Ag/Au nanodecahedra.

In the growth process, Ag nanoparticles adhere to form clusters, then the formation of Ag nanodecahedra from these clusters is controlled by the lowest surface energy. The different crystalline planes of Ag feature different surface energies in the sequence $\{111\} < \{100\} < \{110\}$ for FCC crystals [8].

Figure 6 shows the distribution of Ag and Au elements in the sample performed by EDX elemental mapping. From the pseudo-colored EDX mapping images, it can be seen that the Ag elements (green) are mainly distributed on the cores, and the Au elements (red) are mainly distributed on the shell layers, exhibiting a well-synthesized and stabilized coverage. The corresponding elemental maps indicate the expected homogeneously spatial distribution of Ag and Au on the entire volume of the nanodecahedra. The formed nanodecahedra shows obvious core-shell structures, and the boundary between the hollow core and the shell layer is clear.

EDS result revealed only Au and Ag signals of Ag/Au nanodecahedra sample (Fig. 6e). The peaks of Ag and Au were 2.16 keV and 9.6 keV, respectively. The Au peak intensity of samples increased with the $HAuCl_4$ amount increase (data not shown here). Au and Ag have the same crystal structure lattice constant, so Au can be densely deposited on Ag cores with smooth surface coverage.

3.3. UV-Vis Spectra

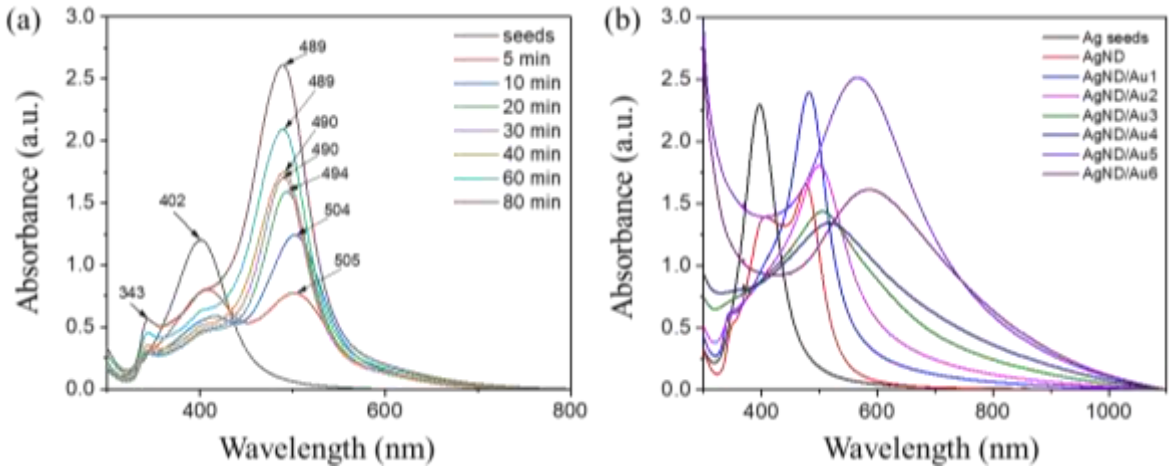

Figure 7. UV-Vis spectra of (a) AgND, (b) Ag/Au bimetallic nanodecahedra.

Fig. 7a illustrates the ultraviolet-visible-near infrared light (300 - 800 nm) absorption spectra of Ag seeds and various AgND samples under different BLED illumination times (5-80 min). The intensity of 400 nm peak decreased with increased BLED illumination time. The edge in the 500 nm peak blue-shifted as the BLED illumination time increased. The larger dimension of AgND enhanced the plasmonic response of the Ag core. The UV-Vis spectra revealed the plasmonic response of the light-illuminated material. Two optical plasma wavelengths of Ag are of 400 nm and 500 nm. The plasma wavelength of Ag/Au composited material can be tuned using different component ratios.

Ascorbic acid is a mild reducing agent widely used in the synthesis of metallic gold nanostructure. According to Eq. (2), for $HAuCl_4$ to react completely with AA, the molar ratio of AA and $HAuCl_4$ should be greater than 6:1. In our experiment, we added 0.4 ml of 0.01 M L-AA (4 µmol) while keeping the volume of $HAuCl_4$ solution added constant at 10 µl and changing only the molar number of $HAuCl_4$ while keeping other synthetic conditions constant. The maximum amount of $HAuCl_4$ required to be completely reduced is 0.6 µmol. From Fig. 7b, one can see that the absorption peak of the Ag/Au1 is located at 510 nm after adding 0.15 µmol $HAuCl_4$ and monotonically red-shifted to 530 nm, 550 nm,

570 nm, 590 nm, and 610 nm after adding 0.25, 0.35, 0.45, 0.55, and 0.65 µmol of $HAuCl_4$, respectively. The addition of $HAuCl_4$ amount resulted in a red-shift of the plasmonic resonance peak in the absorption spectra due to the increased content of elemental Au in the products and the enhancement of the plasmon coupling between the nanodecahedra. When the amount of $HAuCl_4$ was increased, the rate of the reduction reaction increased, and more Au monomers were produced at the same time. The half-peak width of the absorption peak increased because the larger the amount of $HAuCl_4$, the faster the reaction rate between L-AA and $HAuCl_4$, and the more Au is generated under the same reaction time, so the particle size of the nanodecahedra increased. When the amount of $HAuCl_4$ reached 0.65 µmol, $HAuCl_4$ was in excess, the thickness of the Au nanolayer reached maximum, and the position and width of the absorption peak stopped shifting.

3.4. The Synthesis Mechanism of Ag/Au Nanodecahedra

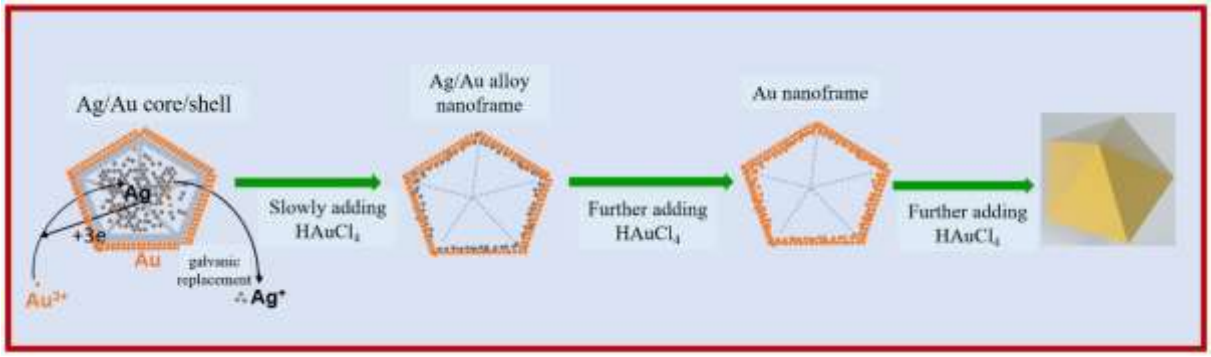

Figure 8. The synthesis mechanism of Ag/Au nanodecahedra via galvanic replacement process.

The synthesis of Ag/Au nanodecahedra is mainly divided into two stages. In the first stage, AgND with uniform size and good dispersion was prepared by photochemical reaction. In the second stage, L-AA was used to reduce $HAuCl_4$ on the surface of AgND, forming Ag/Au bimetallic nanodecahedra. The standard redox potential of $AuCl_4^- / Au$ is 0.99 V [21] and that of Ag^+/Ag is 0.8 V [22]. A galvanic replacement reaction occurred with the following equation [23]:

$$3Ag(s) + HAuCl_4(aq) \rightarrow Au(s) + 3AgCl(s) + HCl(aq) \quad (1)$$

Three Ag atoms are consumed to produce one Au atom, so Ag is consumed three times faster than the subsequent deposition of Au^0 [24]. Au^{3+} ions gained electrons from Ag atoms and were reduced to Au^0 atoms which were deposited on the surface of AgND and evolved into a shell-like structure through the Ostwald ripening process [25]. Simultaneously, the silver template was consumed, and the morphology of the nanodecahedra changed from nanoshells with partially hollow cores (Ag/Au alloy nanoframe) to completely hollow cores (Au nanoframe) with further adding $HAuCl_4$ (Fig. 8).

4. Conclusions

In summary, high-density Ag nanodecahedra samples were successfully synthesized by using the reduction method followed by a photochemical process using BLED irradiation. The Au nanolayer was coated on the surface of the Ag nanodecahedra by chemical reduction method to obtain Ag/Au bimetallic nanodecahedra. SEM and TEM images showed that the diameter of the products was of ca. 80 nm. The optical property of Ag and Ag/Au nanodecahedra is greatly affected by BLED illumination time and

$HAuCl_4$ amount. The size of AgND increased as BLED illumination time increased. The $HAuCl_4$ amount has an impact on the rate of Au deposition. The UV-Vis absorption spectra revealed the blue-shift of the Ag absorption peak as the BLED illumination time increased from 5 to 80 min and the red-shift of Ag/Au absorption peak as the Au amount increased.

Acknowledgements

The authors would like to acknowledge the financial support of ĐT CTVL 2021-2025 under grant number ĐTĐLCN.23/23.

References

[1] J. K. Kim, T. H. Park, D. J. Jang, Surface-Enhanced Raman Scattering and Photothermal Effect of Hollow Au Nanourchins with Well-Defined Cavities, J. Nanopart. Res., Vol. 22, No. 305, 2020, pp. 1-11, https://doi.org/10.1007/s11051-020-05034-y.

[2] B. Klębowski, J. Depciuch, M. P. Wojtan, J. Baran, Applications of Noble Metal-Based Nanoparticles in Medicine, Int. J. Mol. Sci., Vol. 19, No. 12, 2018, pp. 4031, https://doi.org/10.3390/ijms19124031.

[3] O. V. Dement'eva, M. E. Kartseva, Noble Metal Nanoparticles in Biomedical Thermoplasmonics, Colloid J., Vol. 85, No. 4, 2023, pp 500-519, https://doi.org/10.1134/S1061933X23700187.

[4] N. L. Netzer, C. Qiu, Y. Zhang, C. Lin, L. Zhang, H. Fong, C. Jiang, Gold–Silver Bimetallic Porous Nanowires for Surface-Enhanced Raman Scattering, Chem. Commun., Vol. 47, No. 34, 2011, pp. 9606-9608, https://doi.org/10.1039/C1CC13641K.

[5] Y. Wang, J. Wan, R. J. Miron, Y. Zhao, Y. Zhang, Antibacterial Properties and Mechanisms of Gold–Silver Nanocages, Nanoscale, Vol. 8, No. 21, 2016, pp. 11143-11152, https://doi.org/10.1039/C6NR01114D.

[6] J. K. Majhi, P. K. Kuiri, Spectral Tuning of Plasmon Resonances of Bimetallic Noble Metal Alloy Nanoparticles through Compositional Changes, Plasmon, Vol. 15, No. 3, 2020, pp. 797-804, https://doi.org/10.1007/s11468-019-01103-8.

[7] J. K. Majhi, P. K. Kuiri, Enhancement of Spectral Shift of Plasmon Resonances in Bimetallic Noble Metal Nanoparticles in Core–Shell Structure, J. Nanopart. Res., Vol. 22, No. 4, 2020, pp. 86, https://doi.org/10.1007/s11051-020-4782-0.

[8] H. J. Yin, Z. Y. Chen, Y. M. Zhao, M. Y. Lv, C. A. Shi, Z. L. Wu, X. Zhang, L. Liu, M. L. Wang, H. J. Xu, Ag@Au Core-Shell Dendrites: A Stable, Reusable and Sensitive Surface Enhanced Raman Scattering Substrate, Sci. Rep., Vol. 5, No. 1, 2015, pp. 14502, https://doi.org/10.1038/srep14502.

[9] H. J. Huang, M. H. Shiao, Y. W. Lin, B. J. Lin, J. Su, Y. S. Lin, H. W. Chang, Au@Ag Dendritic Nanoforests for Surface-Enhanced Raman Scattering Sensing, Nanomater, Vol. 11, No. 7, 2021, pp. 1736, https://doi.org/10.3390/nano11071736.

[10] Y. Yang, J. Shi, G. Kawamura, M. Nogami, Preparation of Au–Ag, Ag–Au Core–Shell Bimetallic Nanoparticles for Surface-Enhanced Raman Scattering, Scr. Mater., Vol. 58, No. 10, 2008, pp. 862-865, https://doi.org/10.1016/j.scriptamat.2008.01.017.

[11] X. H. Pham, M. Lee, S. Shim, S. Jeong, H. M. Kim, E. Hahm, S. H. Lee, Y. S. Lee, D. H. Jeong, B. H. Jun, Highly Sensitive and Reliable SERS Probes Based on Nanogap Control of a Au–Ag Alloy on Silica Nanoparticles, RSC Adv., Vol. 7, No. 12, 2017, pp. 7015-7021, https://doi.org/10.1039/C6RA26213A.

[12] Y. F. Fu, J. Zhu, X. Li, G. J. Weng, J. J. Li, J. W. Zhao, Au-Ag Nano-Garlands as a Versatile SERS Substrate: Two-Step Synthesis Realizes the Growth of Petal-Shaped Branches on Hollow Au-Ag Nanoshells, Colloids Surf, A: Physicochem. Eng. Aspects, Vol. 698, 2024, pp. 134541, https://doi.org/10.1016/j.colsurfa.2024.134541.

[13] Y. Liu, Z. Qin, X. Jia, J. Zhou, H. Li, X. Wang, G. Wang, Direct Detection of Polystyrene Microspheres by Using Easily Fabricated Ag Core Embedded Au Film SERS Substrates with High Sensitivity, J. Environ. Chem. Eng., Vol. 12, No. 5, 2024, pp. 113311, https://doi.org/10.1016/j.jece.2024.113311.

[14] A. Kohut, A. Kéri, V. Horváth, J. Kopniczky, T. Ajtai, B. Hopp, G. Galbács, Z. Geretovszky, Facile and Versatile Substrate Fabrication for Surface Enhanced Raman Spectroscopy Using Spark Discharge Generation of Au/Ag Nanoparticles, Appl. Surf. Sci., Vol. 531, 2020, pp. 147268, https://doi.org/10.1016/j.apsusc.2020.147268.

[15] G. A. Khan, O. Ö. Demirtaş, A. Bek, A. S. Bhatti, W. Ahmed, Facile Fabrication of Au-Ag Alloy Nanoparticles on Filter Paper: Application in SERS based Swab Detection and Multiplexing, Vib. Spectrosc., Vol. 120, 2022, pp. 103359, https://doi.org/10.1016/j.vibspec.2022.103359.

[16] S. H. Lee, I. B. Ansah, C. Mun, J. Y. Yang, S. Y. Shin, J. Na, J. Park, S. Y. Nam, S. Lee, J. Kim, Galvanic Engineering of Interior Hotspots in 3D Au/Ag Bimetallic SERS Nanocavities for Ultrasensitive and Rapid Recognition of Phthalate Esters, Chem. Eng. J., Vol. 470, 2023, pp. 144161, https://doi.org/10.1016/j.cej.2023.144161.

[17] Y. C. Liu, S. J. Yang, Improved Surface-Enhanced Raman Scattering Based on Ag–Au Bimetals Prepared by Galvanic Replacement Reactions, Electrochim. Acta, Vol. 52, No. 5, 2007, pp. 1925-1931, https://doi.org/10.1016/j.electacta.2006.07.057.

[18] J. M. Park, H. E. Choi, D. Kudaibergen, J. H. Kim, K. S. Kim, Recent Advances in Hollow Gold Nanostructures for Biomedical Applications, Front. Chem., Vol. 9, 2021, pp. 699284, https://doi.org/10.3389/fchem.2021.699284.

[19] J. Emsley, The Elements, Oxford University Press, 1998.

[20] V. X. Hoa, N. D. Dien, P. T. T. Ha, N. V. Truong, N. X. Ca, V. V. Thu, Tunable LSPR of Silver/Gold Bimetallic Nanoframes and Their SERS Activity for Methyl Red Detection, RSC Adv., Vol. 11, No. 24, 2021, pp. 14596-14606, https://doi.org/10.1039/D1RA01477C.

[21] J. Zhu, S. Zhang, G. J. Weng, J. J. Li, J. W. Zhao, The Morphology Regulation and Plasmonic Spectral Properties of Au@AuAg Yolk-Shell Nanorods with Controlled Interior Gap, Spectrochim. Acta Part A: Mol. Biomol. Spectrosc., Vol. 236, 2020, pp. 118343, https://doi.org/10.1016/j.saa.2020.118343.

[22] B. R. González, A. Burrows, M. Watanabe, C. J. Kiely, L. M. L. Marzán, Multishell Bimetallic AuAg Nanoparticles: Synthesis, Structure and Optical Properties, J. Mater. Chem., Vol. 15, No. 17, 2005, pp. 1755-1759, https://doi.org/10.1039/B500556F.

[23] S. G. Jiji, K. G. Gopchandran, Au–Ag Hollow Nanostructures with Tunable SERS Properties, Spectrochim. Acta Part A: Mol. Biomol. Spectrosc., Vol. 171, 2017, pp. 499-506, https://doi.org/10.1016/j.saa.2016.08.022.

[24] C. H. Tsai, S. Y. Chen, J. M. Song, M. Haruta, H. Kurata, Effect of Ag Templates on the Formation of Au-Ag Hollow/Core-Shell Nanostructures, Nanoscale Res. Lett., Vol. 10, 2015, pp. 438, https://doi.org/10.1186/s11671-015-1141-7.

[25] A. R. Roosen, W. C. Carter, Simulations of Microstructural Evolution: Anisotropic Growth and Coarsening, Phys. A: Stat. Mech. Appl., Vol. 261, No. 1-2, 1998, pp. 232-247, https://doi.org/10.1016/S0378-4371(98)00377-X.